Dual-Site Supported Metallocene Catalyst Design for Bimodal Polyolefin Synthesis

Phillip Hamilton, Hao Song, and Dan Luss
Dept. of Chemical and Bimolecular Engineering, Univ. of Houston, Houston, TX 77204

DOI 10.1002/aic.11094
Published online January 19, 2007 in Wiley InterScience (www.interscience.wiley.com).

The processability of various polyolefins may be enhanced by producing one having a bimodal molecular weight distribution. Such polymers can be produced by loading the reactor with a catalyst on which two different catalytic sites are impregnated. The catalysts must be loaded with a proper ratio between the two catalytic sites to produce the desired polymer. The total loading should enable a maximum polymer production in the specified residence time while keeping the maximum transient temperature below a specified maximum, in order to avoid local melting and sheet formation. A model is presented that enables this catalyst design based on kinetic information about the initiation, propagation, and deactivation reaction rates of the two individual catalytic sites. The model simulations provide insight about the factors affecting the maximum safe loading of the two catalytic sites. We show here how to utilize kinetic information about each of the two catalytic sites to predict the optimum loading of dual-site metallocene catalysts. As the maximum temporal temperature occurs during the initial stages of the reaction, the site that leads to a faster generation of a temperature peak, exerts a stronger bound on the total polymer production than the second site. The larger the propagation and/or the initiation rate constants or their activation energies are, the lower should be the catalyst loading. The deactivation rate constants affect both the relative site loading of the two sites as well as the total production. The total polymer production can be increased by decreasing the deactivation rate of the more active site. © 2007 American Institute of Chemical Engineers *AIChE J,* 53: 687–694, 2007
Keywords: bimodal polyolefins, metallocene catalysts, temperature rise, catalyst design, dual-site catalyst

Introduction

Metallocene catalysts enable control of polymer structure, to create polymers with desired physical properties[1] and to manufacture improved polymers. For example, they have been utilized to produce previously unobtainable stereo-regular polypropylenes, syndotactic polystyrene, ethylene-styrene copolymers, and block copolymers. The metallocene catalysts can also produce polymers of higher molecular weight and narrower molecular weight distribution than conventional Ziegler-Natta catalysts.[2] Polymers produced by single site catalysts have good mechanical properties due to their narrow molecular weight distribution (MWD) but are difficult to process.[3–7] The processing and mechanical properties can often be enhanced by synthesizing a polymer having a bimodal MWD, as they have a better balance between rheological behavior and final mechanical properties than polymers with a unimodal MWD. The processability of a physical mixture of two polymers can suffer from inhomogeneous distribution of the two polymers. Thus, the synthesis of these bimodal polymers is usually conducted in situ in a sequence of two or more reactors.[8,9] A recent advance is the production of a bimodal polymer in a single reactor using a dual site catalyst, that is, one on which two different metallocene catalysts are impregnated on the support.[10–12]

Industrial experience revealed that olefins gas-phase polymerization by metallocene catalysts in fluidized-bed reactors can lead to local overheating of the growing polymer particles. When

Current address of H. Song: Dept. of Biomedical Engineering, Duke Univ., Durham NC 27708.
Correspondence concerning this article should be addressed to D. Luss at dluss@uh.edu.

a growing particle softens or melts, other particles stick to it, eventually forming polymer "sheets" that require reactor shutdown and loss of production time. These technical problems compelled Exxon to declare *force majeure* on its Exceed line of metallocene LLDPE catalysts at the Mont Belvieu plant in 1997, which was the first commercial, gas-phase polyolefin polymerization by metallocene catalysts. To develop catalysts that avoid sheet formation, it is important to understand the mechanisms involved and to be able to predict the conditions that lead to the local overheating.[13] Many studies investigated the temperature rise during gas-phase olefin polymerization.[14–20] The early mathematical models accounted only for the polymer chain propagation reaction.[14–19] Song and Luss[20] showed that a proper prediction of the temperature rise during the polymerization requires accounting also for the chain initiation and catalyst deactivation.

In order to produce a bimodal polymer with a specified MWD, the catalyst support should be impregnated with a proper ratio between the two catalytic sites. We present here guidance on how dual-site catalysts should be loaded so that they produce the highest possible amount of the desired polymer while keeping the transient temperature below a specified maximum temperature. This study is an extension of a previous one associated with the design of single-site metallocene catalysts.[14–20] We predict the optimum loading of dual-site metallocene catalysts utilizing the kinetic information about each of the two catalytic sites.

Model Development

Gas-phase olefin polymerization may be described by the simplified reaction network[20]:

$$C^0 \xrightarrow{k_i} C^* \xrightarrow{k_p} C^*(p_j) \quad (j = 1, 2, \ldots)$$
$$\searrow \quad \swarrow$$
$$k_d \qquad k_d$$

Deactitvated Catalyst

where C^0 is the total concentration of the deposited catalyst sites, C^* the concentration of active sites to which no polymer chain is attached, $C^*(p_j)$ the concentration of active sites with an attached living polymer with chain length *j, and* $\overline{C^*} = \sum_{j=0}^{\infty} C^*(p_j)$ the total concentration of the active sites. We describe the polymer production rate and heat evolution using a lumped-thermal, uniformly distributed catalyst model. We assume that the catalyst site concentration remains uniform as the polymer particle grows and that the particle temperature is uniform, but different from that of the ambient gas. We account for intra-particle monomer concentration gradients by an isothermal effectiveness factor. The dual-site model considers two types of active sites denoted as site 1 and site 2. The initial concentration of sites 1 and 2 are C_1^0 (0) and C_2^0 (0), respectively. The governing equations are:

$$\frac{dM}{dt} = k_c a_v (M_b - M) - \eta M \sum_{j=1}^{j=2} k_{pj}(T_p)\overline{C_j^*}, \tag{1}$$

$$\rho_p c_p \frac{dT_p}{dt} = h_f a_v (T_b - T_p) + \eta M \sum_{j=1}^{j=2} (-\Delta H_j) k_{pj}(T_p)\overline{C_j^*}, \tag{2}$$

$$\frac{d(\overline{C_j^*}V_p)}{dt} = \left[k_{ij}(T_p)C_j^0 - k_{dj}(T_p)\overline{C_j^*}\right]V_p \quad (j = 1, 2), \tag{3}$$

$$\frac{d(C_j^0 V_p)}{dt} = -k_{ij}(T_p)\, C_j^0 V_p \quad (j = 1, 2), \tag{4}$$

$$\frac{dV_p}{dt} = \frac{M_w}{\rho_p}\eta V_p M \sum_{j=1}^{j=2} k_{pj}(T_p)\overline{C_j^*}, \tag{5}$$

where

$$\eta = \frac{3(\psi \coth\psi - 1)}{\psi^2}, \tag{6}$$

$$\psi = R\sqrt{\frac{\sum_{j=1}^{j=2} k_{pj}(T_p)\overline{C_j^*}}{D_e}}, \tag{7}$$

and

$$k_{lj}(T_p) = k_{lj}(T_b)\exp\left[\frac{\Delta E_{lj}}{R_g}\left(\frac{1}{T_b} - \frac{1}{T_p}\right)\right], \quad (1 = i, p, d), (j = 1, 2). \tag{8}$$

The corresponding initial conditions are:

$$M = \overline{C_1^*} = \overline{C_2^*} = 0,\ T_p = T_b,\ C_1^0 = C_1^0(0),$$
$$C_2^0 = C_2^0(0),\ \mathrm{V_p} = \mathrm{V_p}(0), \qquad \text{at} \quad t = 0. \tag{9}$$

Floyd et al.[21] pointed out that the gas Sherwood number is constant for the typically low Reynolds numbers of the small growing polymer particles. We define the dimensionless variables and parameters,

$$x = \frac{M}{M_b}, \quad y = \frac{T_p}{T_b}, \quad g_r = \frac{R}{R(0)}, \quad \tau = \frac{t}{R(0)^2/D_e},$$
$$x_{*j} = \frac{\overline{C_j^*}}{C_j^{\mathrm{Ref}}}, \quad x_{0j} = \frac{C_j^0}{C_j^{\mathrm{Ref}}}, \quad w_j = \frac{C_j^0(0)}{C_j^{\mathrm{Ref}}},$$
$$\gamma_{lj} = \frac{\Delta E_{lj}}{R_g T_b}, \quad \phi_{pj} = R(0)\sqrt{\frac{k_{pj}(T_b)C_j^{\mathrm{Ref}}}{D_e}}, \quad \phi_{ij} = R(0)\sqrt{\frac{k_{ij}(T_b)}{D_e}},$$
$$\phi_{dj} = R(0)\sqrt{\frac{k_{dj}(T_b)}{D_e}}, \quad B_{im} = \frac{k_c(0)R(0)}{D_e}, \quad \beta_j = \frac{(-\Delta H_j)k_c(0)M_b}{h_f(0)T_b},$$
$$Le = \frac{\rho_p c_p k_c(0)}{h_f(0)}, \quad p = \frac{M_w M_b}{\rho_p} \tag{10}$$

where j = 1,2 and C_j^{Ref} is the concentration of active sites of type j, loaded on the catalyst in the experiments used to determine the values of $k_{pj}(T_b)$. The dimensionless model equations are:

$$\frac{dx}{d\tau} = \frac{3B_{im}}{g_r^2}(1 - x) - \eta \sum_{j=1}^{2} \phi_{pj}^2 \exp[\gamma_{pj}(1 - 1/y)]xx_{*j} \tag{11}$$

$$Le\frac{dy}{d\tau} = \frac{3B_{im}}{g_r^2}(1 - y) + \eta \sum_{j=1}^{2} \phi_{pj}^2 \beta_j \exp[\gamma_{pj}(1 - 1/y)]xx_{*j} \tag{12}$$

$$\frac{dx_{*j}}{d\tau} = \phi_{ij}^2 \exp[\gamma_{ij}(1-1/y)]x_{0j} - \phi_{dj}^2 \exp[\gamma_{dj}(1-1/y)]x_{*j} - p\eta \sum_{h=1}^{2} \phi_{ph}^2 \exp[\gamma_{ph}(1-1/y)]xx_{*h}^2 \quad (j=1,2) \tag{13}$$

$$\frac{dx_{0j}}{d\tau} = -\phi_{ij}^2 \exp[\gamma_{ij}(1-1/y)]x_{0j} - p\eta \sum_{h=1}^{2} \phi_{ph}^2 \exp[\gamma_{ph}(1-1/y)]xx_{*h}x_{0h} \quad (j=1,2) \tag{14}$$

$$\frac{dg_r}{d\tau} = p\frac{g_r}{3}\eta \sum_{j=1}^{2} \phi_{pj}^2 \exp[\gamma_{pj}(1-1/y)]xx_{*j} \tag{15}$$

where

$$\eta = \frac{3(\psi \coth\psi - 1)}{\psi^2} \tag{16}$$

and

$$\psi = g_r \sqrt{\sum_{j=1}^{2} \phi_{pj}^2 \exp[\gamma_{pj}(1-1/y)]x_{*j}} \tag{17}$$

As the particle grows, dilution decreases the uniform concentration of the catalytic sites by a factor of g_r^{-3}. Thus, the Thiele modulus, ψ, is proportional to $g_r^{-0.5}$, and the value of the isothermal effectiveness factor is shifted towards unity as the particle grows. The corresponding initial conditions are:

$$x = x_{*1} = x_{*2} = 0, \quad y = 1, \quad x_{01} = w_1, \quad x_{02} = w_2, \quad g_r = 1, \quad \tau = 0 \tag{18}$$

Equations 9–18 were used to simulate the polymerization in a dual-site metallocene catalyst. The time-average of the polymer production P_j (j = 1,2) by site j is:

$$\langle P_j \rangle = \int_0^{t_f} k_{pj}(T_p)\overline{C_j^*}\,\mathrm{MV}_p\eta\,\mathrm{d}t/t_f \qquad (j=1,2). \tag{19}$$

We define a dimensionless production, P_j, as:

$$P_j = \frac{\langle P_j \rangle}{V_p(0)M_b} \qquad (j=1,2). \tag{20}$$

The total dimensionless production by the two sites is $P = P_1 + P_2$.

The set of algebraic-differential equations was solved by the Limex solver.[22] We define a *maximum temperature set*, to be the parameters at which the maximum transient particle temperature attains a specified value. This maximum transient temperature must be lower than the melting one, to avoid polymer particles sticking to each other and formation of large agglomerates (sheeting). Clearly, the model is not valid for temperatures exceeding the melting temperature, as it does not account for the polymer melting. The melting set, as defined by Song and Luss,[14] is the maximum temperature set when we select the melting temperature of the polymer as the maximum allowable temperature.

The loading of the catalyst by the two sites depends on the kinetic features of the sites. When both have similar kinetic behavior, that is, when similar temporal temperature rise occurs when only one of the sites is impregnated on the support, then one can treat the temperature rise as generated by a single "lumped" reaction. In such cases, the total loading of the active sites can be handled by the procedure described by Song and Luss[14] for the case of a single reaction, just using the model presented here to determine the ratio between the two sites that produces the desired bimodal MWD. We consider here the more general cases in which the temporal temperature rise generated by the two sites are different so that the heat generation cannot be properly described by a lumped single-reaction model.

Model Predictions

Simulations were conducted to determine the loading of dual-site catalysts that produce, during a specified period (1 h in our simulations), the largest time-average amount of the desired bimodal polymer (with a specified ratio between the two products), while keeping the maximum transient temperature below a specified maximum temperature ($T_{\max} = T_m$). In all the simulations reported here, the loading of the two sites was adjusted so that an equal amount of the two products, P_1 and P_2, was produced. Typical ranges of values of the physical parameters encountered in gas-phase olefin polymerization are: $R(0)$ = 5-50 μm; k_p(353 K) = 60-1500 s^{-1}; k_i(353 K) = 5-50 hr^{-1}; k_d(353 K) = 0.5-20 hr^{-1}; ΔE_p, ΔE_i, and ΔE_d = 12-65 KJ/mol; D_e = 0.00008-0.0005 cm^2/s; M_b = 0.0004-0.0012 mol/cm^3; T_b = 343-353 K; $(-\Delta H) \sim$ 108 KJ/mol (propylene); $(-\Delta H) \sim$ 104 KJ/mol (ethylene); λ_f = 0.00012-0.0003 J/(cm*s*K); λ_e = 0.0008-0.002 J/(cm*s*K); and $\rho_p c_p \sim$ 1.26 J/(cm^3*K).[14–21,23–28]

From these physical parameters ranges, ranges of the dimensionless parameters can be determined. Typical ranges of values of the dimensionless parameters encountered in gas-phase olefin polymerization are: γ_p, γ_i, and γ_d = 4-20; ϕ_p = 0.5-5; ϕ_i = 0.004 -0.04; ϕ_d = 0.0005-0.02; β = 2-6.5; Bi_m = 10-60; Bi_h = 0.1-0.3; Le = 5-30; and p = 0.01-0.03. The values of the parameters used in the simulations were within these ranges. The base set of typical parameters values for the two sites were:

$$\phi_{p1} = 4, \quad \phi_{p2} = 2, \quad \gamma_{p1} = 14, \quad \gamma_{p2} = 7,$$
$$\phi_{i1} = 0.02, \quad \phi_{i2} = 0.01, \quad \gamma_{i1} = \gamma_{i2} = 14,$$
$$\phi_{d1} = 0.002, \quad \phi_{d2} = 0.001, \quad \gamma_{d1} = \gamma_{d2} = 7,$$
$$\beta_1 = \beta_2 = 2, \quad B_{im} = 20, \quad \mathrm{Le} = 25, \quad p = 0.019.$$

Figure 1 shows that when only one site is impregnated on the support, catalytic site 1 reaches its peak temperature at 1/3 of the time it takes site 2. Hence, we refer to site 1 as the more active one.

The simulated values of the temporal temperature, effectiveness factor, and particle dimensionless radius are shown in Figure 2 using the base set of parameter values. In all the simulations, we assume that an equal amount of polymer is produced by the two sites, that is, $P_1 = P_2$. The simulations show that the catalyst particle temperature increased rapidly after the beginning of the reaction and reached its maximum value within a rather short time relative to a typical sojourn in the reactor (order 1-3 h), and it then cooled down to a temperature close to that of the bulk. Thus, the particle temperature was rather close to that of the ambient gas during a large fraction of

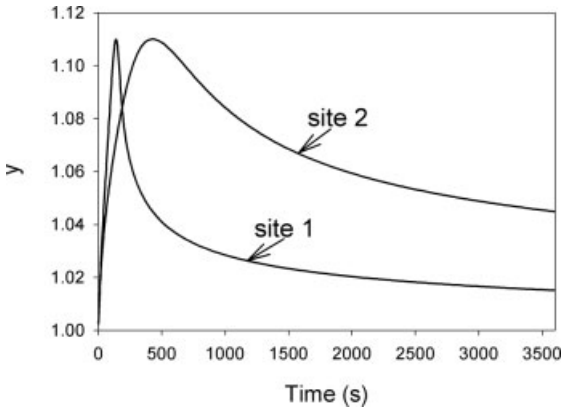

Figure 1. The temporal temperature of a growing polymer particle when only one active site is loaded on the support.

its sojourn in the fluidized bed. Since the particle temperature rise is for such a brief period relative to the entire reaction time, it can be assumed that this temperature rise will have very little effect on the polymer properties. The initial temperature rise caused the Thiele modulus to exceed unity and the corresponding effectiveness factor to be smaller than unity. As the particle grew, the effectiveness factor increased due to the decrease in the temperature and the dilution of the concentration of the active sites in the expanding particle.

Figure 3 shows that the time-average polymer production is essentially proportional to the total catalyst loading ($w_1 + w_2$). The maximum transient temperature is a monotonic increasing function of this loading. In this specific example, the average polymer dimensionless production rate is approximately 700,000 when the maximum dimensionless transient particle temperature is restricted to be 1.11. Similar simulations were used to determine the dependence of the maximum catalyst loading on various kinetic parameters under the constraint that the maximum transient temperature does not exceed the specified maximum.

Simulations were conducted to determine the ratio between the loading of the two sites in order to produce the desired polymer blend. (In this example, the goal is that each site produces an equal amount of polymer). The simulations shown in Figure 4 indicate that the proper ratio between the loading of the two catalytic sites is essentially independent of the total catalyst loading.

Extensive simulations were conducted in order to gain an understanding of the impact of the various kinetic parameters on the optimal loading of the two catalytic sites. The simulations show that the peak transient temperature is a monotonic increasing function of the activation energy of the propagation rate constant of the more active site. However, this activation energy has a very minor impact on the temperature after the rather short period during which the peak temperature exists. Figure 5 shows the impact of γ_{p1} for the base case. The peak temperature increase was rather moderate for all $\gamma_{p1} < 16$. A rather drastic increase in the peak temperature occurred as γ_{p1} increased from 16 to 18. An even more drastic peak temperature increase (not shown in Figure 5) occurred upon a further increase of γ_{p1}.

Increasing the initiation rate constant of the more active site (site 1) significantly increased the peak transient temperature and decreased the time during which the temperature peak evolved. However, after this relatively short time during which the peak temperature existed, the temporal temperature was rather insensitive to the value of the initiation rate constant. Figure 6 illustrates this behavior for the base case for several values of ϕ_{i1}, which is proportional to the initiation rate constant of the more active site.

Extensive simulations were conducted to determine the impact of the kinetic parameters on the time-average production under the constraint on the maximum transient temperature. All these simulations were conducted for cases in which one site is more active than the other, that is, when only one of the two active sites is impregnated on the support the temperature peak is attained at rather different times. The simulations show that in these cases, the kinetic parameters of the more active site have the main impact on the maximum attainable time-average production. The kinetic parameters of the less active catalyst site exert a much weaker impact on the time-average production. Typical results showing the impact of

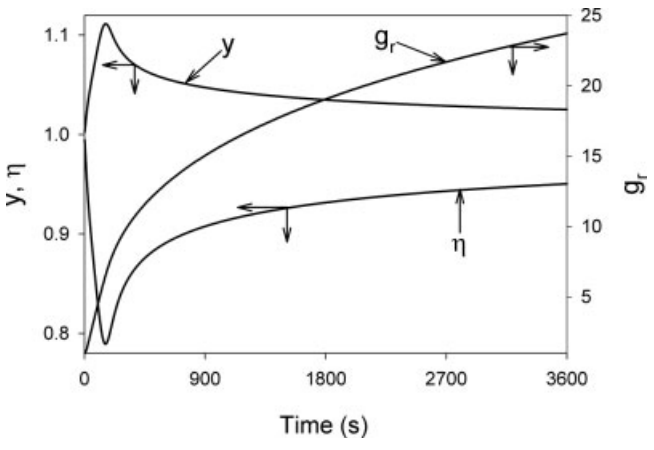

Figure 2. The temporal temperature, effectiveness factor, and growing particle dimensionless radius.

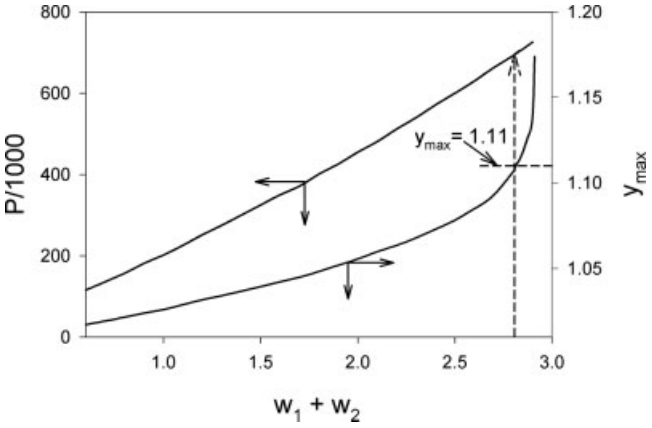

Figure 3. Dependence of the total polymer production and maximum transient temperature on the total loading when each catalytic site produces an equal amount of polymer.

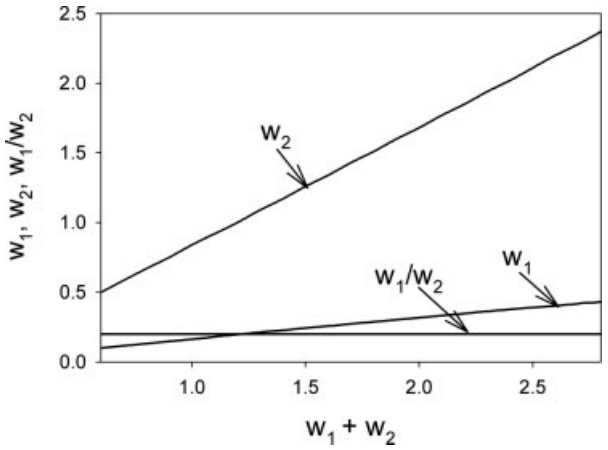

Figure 4. Dependence of the loading of the two catalytic sites and the ratio between them on the total loading when each catalytic site produces an equal amount of polymer.

three kinetic parameters, γ_{p1}, ϕ_{i1}, and ϕ_{d1}, on the maximum time-average polymer production are shown in Figures 7–10.

The time-average production of the polymer is rather sensitive to the value of the activation energy of the propagation rate constant, γ_{p1}, as shown by Figure 7. In contrast, it is rather insensitive to the variation in the value of the propagation rate constant, and is essentially the same for ϕ_{p1} values between 3 and 100. The reason for this is that as ϕ_p is increased, the initial site loading, w, is decreased subject to the maximum temperature constraint. Thus, the time-average production changes very little even with large changes in ϕ_p. The simulations reveal an essentially linear decrease in the time-average production upon an increase in the activation energy. This occurs as the higher the activation energy is, the faster is the increase in the reaction rate upon a temperature change. Hence, a higher temperature peak is obtained for higher values of the activation energy. Thus, in order to keep the temperature peak below the specified maximum, the loading of the catalyst needs to be decreased as the activation energy is increased.

An increase in either the initiation rate constant or its activation energy decreases the maximum possible time-average

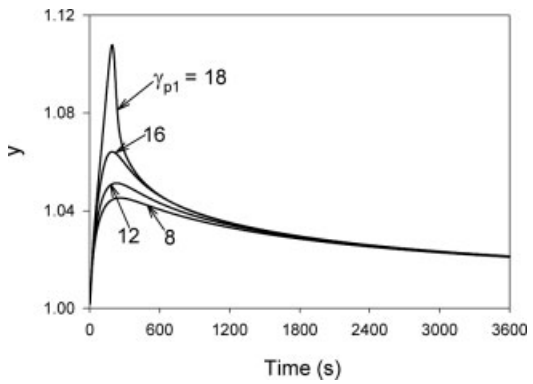

Figure 5. Dependence of the temporal temperature on the activation energy of the propagation rate constant, γ_{p1}.

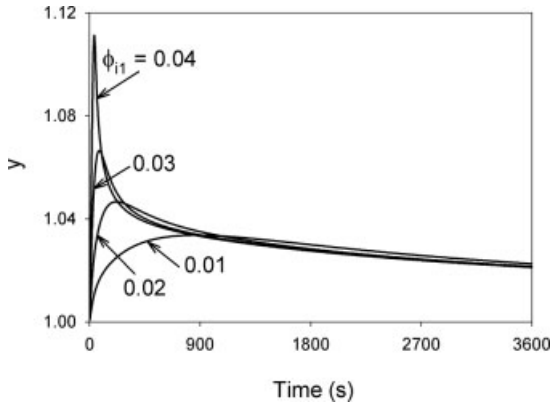

Figure 6. Dependence of the temporal temperature on the initiation rate constant of the more active site.

polymer production, as Figure 8 shows. The reason is that an increase in the initiation rate constant leads to a more rapid initial temperature rise and an increase in the amplitude of the temperature peak. Hence, in order to maintain the maximum temperature rise below the specified maximum, the total loading of the catalyst has to be decreased. This, in turn, decreases the total polymer production.

The rate constant for catalyst deactivation (ϕ_{d1}) has a direct effect on the total production since a catalyst site with a high rate of deactivation will produce polymer for a shorter period than one with a lower deactivation rate. The rate constant for the active site deactivation (ϕ_{d1}) has a strong effect on both the ratio between the loading of the two types of sites as well as on the time-average production rate. Figure 9 shows that $w_1/(w_1 + w_2)$ is a monotonic increasing function of both γ_{d1} and ϕ_{d1}. Figure 10 shows that the time-average production is a monotonic decreasing function of both γ_{d1} and ϕ_{d1}. Thus, the higher the deactivation rate constant of the more active site and/or its activation energy, the higher should be the fraction of that site

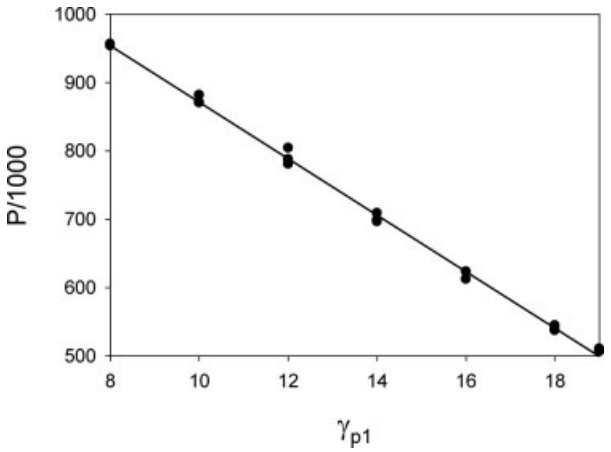

Figure 7. Dependence of the time-average production on the activation energy and rate constant for the propagation reaction on production.

The production rate for each γ_{p1} was computed for various ϕ_{p1} between 3 and 100.

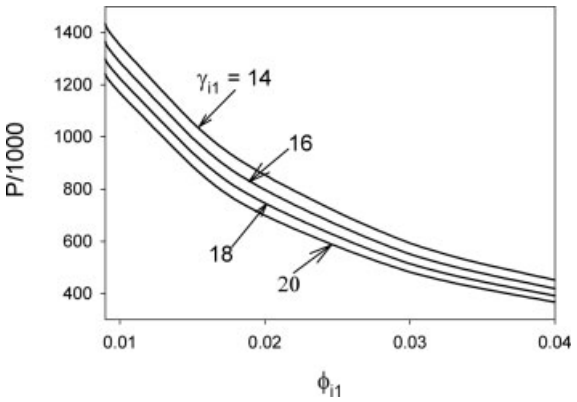

Figure 8. Dependence of the time-average polymer production on ϕ_{i1} and γ_{i1}.

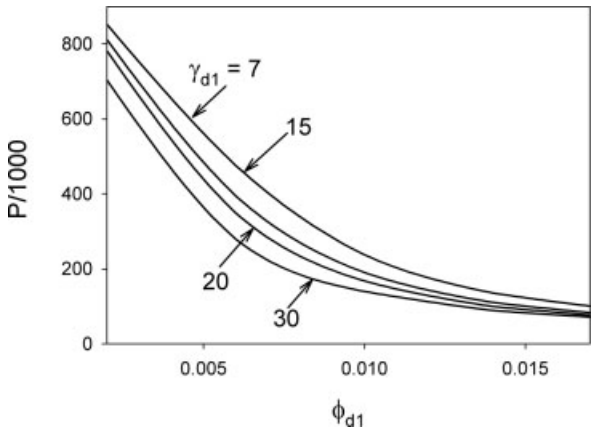

Figure 10. Dependence of the time-average polymer production on ϕ_{d1} and γ_{d1}.

on the catalyst and the lower is the maximum possible time-average production of the polymer subject to the constraint on the maximum temperature.

Simulations showed that initially the ratio between the polymer generated by the two sites (P_1/P_2) was larger than the specified value (Figure 11). However, due to the more rapid decay of the more active sites, the desired ratio was obtained at the end of the specified period (1 h in our simulations). The simulations showed that for a residence time of at least 1 h, this ratio of P_1/P_2 was a rather weak, monotonic decreasing function of the total reaction period.

Discussion

The simulations showed that an increase in the total catalyst loading increased both the total amount of product and the maximum transient catalyst temperature (Figure 3). The total polymer production rate was essentially proportional to the catalyst loading. This occurred as during a large fraction of the polymerization period, the temperature was close to that of the bulk and the diffusional limitations were minimal. The only exception occurred during the relatively short period in which the peak temperature existed. Under these conditions, the total polymer production was approximately proportional to the overall propagation rate constant, which is proportional to the catalyst loading. In contrast, the maximum transient catalyst temperature was rather sensitive to an increase in the catalyst loading, which increased the initial reaction rate. This increased the initial pellet temperature, which increased, in turn, the reaction rate constants, further increasing the temperature. Hence, the percentage increase in the maximum transient temperature exceeded that of the catalyst loading. We point out again that the simulations are not valid for temperatures exceeding the polymer melting, as the model does not account for melting.

The simulations (Figure 4) reveal that in order to maintain a specified ratio between the two polymers (such as $P_1/P_2 = 1$), the ratio between loading of the two catalytic sites, w_1/w_2, should remain approximately constant as the total catalyst loading is increased. Presence of diffusional limitations does not affect this ratio as the effectiveness factor affects equally both polymer production rates. The activation energies of the rate constants of the two propagation reactions are different. Hence, the ratio between the two propagation rate constants varies during the short period in which the particle temperature peak exists. However, this difference in the activation energies is usually rather small and the peak temperature rise is usually rather small (less than 30°C). Thus, this variation in the ratio of

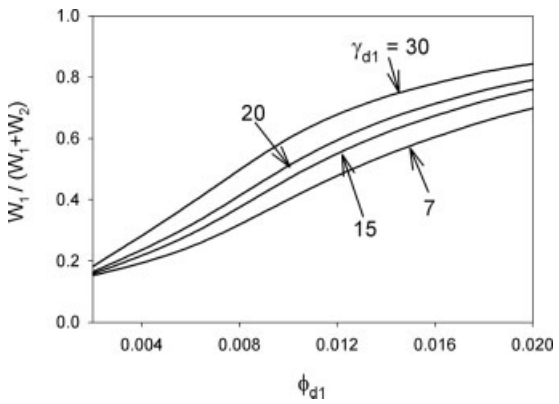

Figure 9. Dependence of the loading ratio $w_1/(w_1 + w_2)$ on ϕ_{d1} and γ_{d1}.

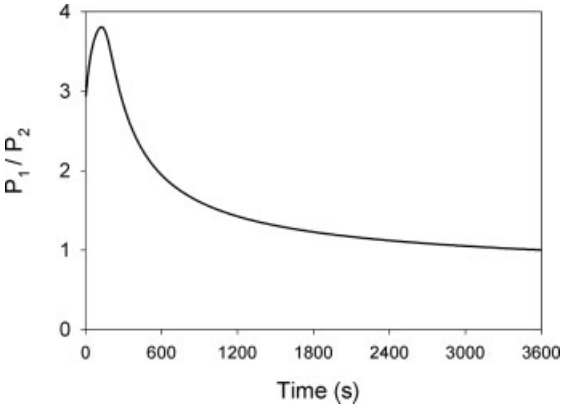

Figure 11. The temporal ratio of polymer produced from each of the two catalytic sites.

the two propagation rate constants is during a small fraction of the particles' sojourn in the reactor. Hence, the ratio between the time average of the two propagation rates is essentially constant for a typical industrial reactor residence time of the order of 1 h (Figure 11). For an average residence time of 1 h (as used in our simulations) or larger, the ratio P_1/P_2 depends on the ratio $(w_1\phi_{p1}^2)/(w_2\phi_{p2}^2)$. Therefore, if the ratio of ϕ_{p1}/ϕ_{p2} remains constant, the ratio of w_1/w_2 must remain constant to produce the specified ratio of P_1/P_2.

The simulations show that the more active catalyst site has a major impact on the maximum catalyst loading and, hence, the time-average production. The temperature spike and the total production are less sensitive to the kinetic features of the less active site than to those of the more active one. The magnitude of the temperature peak is most sensitive to γ_{p1} and ϕ_{i1}, and they affect the magnitude of the safe catalyst loading.

The simulations showed that the time-average production is insensitive to the rate constant of the propagation reaction (Figure 8). The reason is that the total catalyst productivity, which is approximately proportional to the sum of $S = w_1\phi_{p1}^2 + w_2\phi_{p2}^2$, is limited by the constraint that the maximum transient temperature cannot exceed the specified maximum temperature. Thus, a change in the value of the propagation rate constants necessitates a corresponding adjustment in the catalyst loading so that the maximum temperature does not cause melting for the specified ratio of P_1/P_2. Thus, even when the values of ϕ_{p1} and ϕ_{p2} change, the corresponding changes of w_1 and w_2 cause the value of S to remain essentially constant and the time-average catalyst activity remains approximately constant.

An increase in ϕ_{i1} or γ_{p1} increases the transient temperature peak. This requires a reduction in the catalyst loading to maintain the particle temperature below the maximum specified polymer temperature. Thus, the higher the initiation rate constant or the activation energy of the propagation rate constant, the smaller is the total amount of polymer produced subject to the constraint on the maximum temperature rise. The activation energy of the initiation rate constant (γ_{i1}) has a similar effect. However, the total production is more sensitive to ϕ_{i1} than to γ_{i1}. The rate constant for the initiation of site 2 (ϕ_{i2}) also has a similar effect, that is, increasing its value decreases the time-average production. However, the time-average production rate is more sensitive to variations in the value of ϕ_{i1} than to variations of ϕ_{i2}.

The simulations show that a higher deactivation rate of the more active site requires that the support be loaded with a higher percentage of these sites in order to maintain the specified product ratio (Figure 9). This occurs as a catalyst site with a high deactivation rate will produce a polymer for a shorter period than the one with the lower deactivation rate. An increase in the ratio of active sites is required to maintain the specified polymer product composition constraint. Thus, to satisfy simultaneously the constraint on the maximum transient temperature, it is necessary to decrease the total loading of the catalytic sites. This decrease in the loading of the catalyst sites decreases the total amount of polymer produced, as illustrated by Figure 10.

Conclusions

The simulations provide guidance and insight about the loading of silica-supported dual-site metallocene catalysts that maximizes the time-average production of the polymer with the desired composition, while keeping the maximum transient temperature below a specified maximum. We consider here cases in which the time to attain a peak temperature is rather different when the reaction is conducted with a catalyst on which only one of the two sites is impregnated. While the simulations are for a specified product and period of operation, the same methodology can be utilized for the design of many other cases. The insight about the impact of the kinetic features of each of the two sites should be helpful in the design of catalysts that produce desired polymer with a bimodal MWD, while ensuring safe operation and maximizing the total production.

The simulations reveal that when the reaction rate and temperature rise associated with the two sites are rather different, the kinetic features of the more active catalyst site are dominant in controlling the total loading of the catalytic sites subject to the constraint on the maximum temperature rise and the product composition. The temperature peak is most sensitive to the values of γ_{p1} and ϕ_{i1}. In order to avoid exceeding the maximum allowable temperature, the total catalyst loading must be restricted, which, in turn, restricts the time-average production. The time-average production is sensitive to the sum of $w_1\ \phi_{p1}^2 + w_2\ \phi_{p2}^2$. The maximum production corresponds to the highest value of this sum, which still maintains the particle temperature below the maximum allowable temperature rise.

The relative loading of the two sites is controlled primarily by the ratio of ϕ_{p1}/ϕ_{p2} as the specified product ratio, $P_1/P_2 = 1$, is close to being proportional to the ratio $(w_1\phi_{p1}^2)/(w_2\phi_{p2}^2)$. The deactivation rate constants have a significant effect on the relative site loading as well as the total production. The maximum total production can be increased by decreasing the deactivation of the more active site. The modeling and simulation effort presented here offer guidance on how dual-site metallocene catalysts should be loaded so that they attain the highest possible productivity level of the desired polymer product mixture while preventing the transient temperature from exceeding a specified maximum temperature.

Acknowledgments

We are most grateful to Michael E. Muhle for very useful discussions and suggestions and to the ACS-PRF for financial support for the research.

Literature Cited

1. Kaminsky W. New polymers by metallocene catalysis. *Macromol Chem Phys*. 1996;197:3907–3945.
2. Bubeck RA. Structure-property relationships in metallocene polyethylenes. *Mat Sci Eng*. 2002;R 39:1–28.
3. Piel C, Karssenberg FG, Kaminsky W, Mathot VBF. Single-site and dual-site metallocene ethene/propene copolymerizations: experimental and theoretical investigations. *Macromol*. 2005;38:6789–6804.
4. Knuuttila H, Lehtinen A, Salminen H. In: Scheirs J, Kaminsky W. Metallocene Based Polyolefins. Chichester: Wiley; 2000:364–378.
5. Scheirs J, Bohm LL, Boot JC, Leevers PS. *Trends Polym Sci*. 1996; 4:408.
6. Mathot VBF, Pijpers TFJ. PE100 Resins for pipe applications. Continuing the development into the 21st century. *Polym Bull Berlin*. 1984;11:297.
7. Mathot VBF. Crystallization and melting behavior of polyethylene fractions obtained by various fractionation methods. In: Mathot VBF. Calorimetry and Thermal Analysis of Polymers. Munich: Hanser Publishers; 1994: Ch 9.
8. Ahvenainen A, Sarantila K, Andtsjo H, Takakarhu J, Palmroos A. Multistage process for producing polyethylene. U.S. Patent No. 5 326 835;1994.

9. Avela A, Karling R, Takakarhu J. The enhanced bimodal polyethylene technology. *DECHEMA Monogr*. 1998;134:3.
10. Razavi A, Debras GLG. Manufacture of polyolefins with multimodal molecular weight distribution. U.S. Patent No. 5 719 241; 1998.
11. Pettijohn TM. Compositions useful for olefin polymerization and processed therefor and therewith. U.S. Patent No. 5 622 906; 1997.
12. Muhle ME, Sachs WH. Single reactor gas phase process for bimodal products. *Proc Int Conf Polyolefins*. 2004.
13. Rotman D. Metallocene polyolefins: commodity capacity is a reality. *Chem. Week*. 1997;159:20:23.
14. Song H, Luss D. Bounds on operating conditions leading to melting during olefin polymerization. *Ind Eng Chem Res*. 2004;43:270.
15. Hutchinson RA, Ray WH. Polymerization of olefin through heterogeneous catalysis: VII. Particle ignition and extinction phenomena. *J Appl Polym Sci*. 1987;34:657.
16. Zecca JJ, Debling JA. Particle population overheating phenomena in olefin polymerization reactors. *Chem Eng Sci*. 2001;56:4029.
17. Laurence RL, Chiovetta MG. In: Reichert LH, Geisler W. Polymer Reaction Engineering: Influence of Reaction Engineering on Polymer Properties. Munich: Hanser Publishers; 1984:4:73.
18. McKenna TF, Dupuy J, Spitz R. Modeling of transfer phenomena on heterogeneous Ziegler catalysts: differences between theory and experiment in polyolefin (an introduction). *J Appl Polym Sci*. 1995;57:371.
19. McKenna TF, Spitz R, Cokljat D. Heat transfer from catalysts with computational fluid dynamics. *AIChE J*. 1999;45:2392.
20. Song H, Luss D. Impact of initiation and deactivation on melting during gas-phase olefin polymerization. *Ind Eng Chem Res*. 2004;43:4789.
21. Floyd S, Choi KY, Taylor TW, Ray WH. Polymerization of olefins through heterogeneous catalysts: IV. Modeling of heat and mass transfer resistance in the polymer particle boundary layer. *J Appl Polym Sci*. 1986;31:2231.
22. Deuflhar P, Haier E, Zugck J. One step and extrapolation methods for differential-algebraic systems. *Numer Math*. 1987;51:1.
23. Meler GB, Weikert G, Van Swaaij WPM. Gas-phase polymerization of propylene: reaction kinetics and molecular weight distribution. *J Polym Sci A: Polym Chem*. 2001;39:500.
24. Xu ZG, Chakavarti S, Ray WH. Kinetic study of olefin polymerization with a supported metallocene catalyst: I. Ethylene/propylene copolymerization in gas phase. *J Appl Polym Sci*. 2001;80:81.
25. Chakavarti S, Ray WH. Kinetic study of olefin polymerization with a supported metallocene catalyst: II. Ethylene/1-hexene copolymerization in gas phase. *J Appl Polym Sci*. 2001;80:1096.
26. Chakavarti S, Ray WH. Kinetic study of olefin polymerization with a supported metallocene catalyst: III. Ethylene homopolymerization in slurry. *J Appl Polym Sci*. 2001;81:2901.
27. Chakavarti S, Ray WH. Kinetic study of olefin polymerization with a supported metallocene catalyst: IV. Comparison of bridged and unbridged catalyst in gas phase. *J Appl Polym Sci*. 2001;81:1451.
28. Zoellner K, Reichert KH. Gas-phase polymerization of butadiene—kinetics, particle size distribution, modeling. *Chem Eng Sci*. 2001;56:4099.

Manuscript received Sept. 11, 2006, and revision received Dec. 4, 2006.